Non-linear simulations of ELMs in ASDEX Upgrade including diamagnetic drift effects

A. Lessig[1], M. Hölzl[1], F. Orain[1], I. Krebs[1,5], S. Günter[1], E. Franck[4], J. Morales[2], M. Becoulet[2], G. Huysmans[3], M. Dunne[1], ASDEX Upgrade Team[1]

[1] *Max-Planck-Institut für Plasmaphysik, Boltzmannstrasse 2, 85748 Garching, Germany*

[2] *CEA-IRFM, Cadarache, 13108 Saint-Paul-Lez-Durance, France*

[3] *ITER Organization, 13067 Saint-Paul-Lez-Durance, France*

[4] *INRIA Nancy Grand Est, Tonus Team & IRMA, Strasbourg University, France*

[5] *Max-Planck/Princeton Center for Plasma Physics*

Introduction

Edge-localized modes (ELMs) are relaxation-like oscillatory instabilities at the boundary of H-mode plasmas. They eject particles and energy into the scrape-off layer (SOL) on very short time-scales and are driven both by the steep pressure gradient as well as the high bootstrap current in the pedestal region of an H-mode plasma. While they are a mean to control impurity and particle density, extrapolations of experimental data indicate that in devices like ITER the high transient heat loads on plasma-facing components and in particular the divertor targets are beyond the tolerance level of present-day materials. It is therefore important to study ELMs both theoretically and experimentally in order to reveal their fundamental properties which is necessary for the prediction of ELMs and the design of ELM mitigation systems in ITER and DEMO. We present first ELM simulations for ASDEX Upgrade (AUG) including diamagnetic drift effects and investigate the influence of the diamagnetic terms onto the evolution of the toroidal mode spectrum.

Model & Simulations

The model used in our simulations are the reduced resistive MHD equations in toroidal geometry [1] supplemented with ideal wall boundary conditions except for the divertor targets where Bohm boundary conditions are applied. They are solved using the non-linear MHD code JOREK [2, 3]. It uses a flux surface aligned isoparametric Bezier finite element grid in the poloidal plane and a pseudo-spectral discretization in toroidal direction. The flux surface aligned grid is constructed by solving the Grad-Shafranov equation using input-profiles for T, ρ, FF' and $\Psi|_{\text{bnd}}$ created from experimental data using the CLISTE equilibrium reconstruction code [4]. The time stepping is fully implicit leading to large sparse matrices which have to be solved in each time step causing a high memory consumption. This is particularly true for many toroidal harmonics and low resistivity which requires a high grid resolution to resolve the thin current structures formed during an ELM.

Simulation Results

Full ELM crash in AUG

In this section, we present a simulation of a full ELM crash in AUG without diamagnetic drift effects ($\tau_{IC} = 0$). The simulation is based on a typical ELMy H-mode discharge (shot #29342@4.25s) and involves a large number of toroidal harmonics (n=1-22). This allows to study the non-linear evolution of the ELM but (as mentioned above) requires a very large amount of CPU memory which limits the resolution of the poloidal grid and the accessible values for the resistivity. In the simulation at hand the core resistivity is 2.5×10^{-7} Ωm which is approximately one order of magnitude larger than the realistic Spitzer value. Figure 1 shows the time evolution of the normalized magnetic energy for the different toroidal harmonics. At the onset of the ELM high toroidal mode numbers are clearly dominant whereas for later times

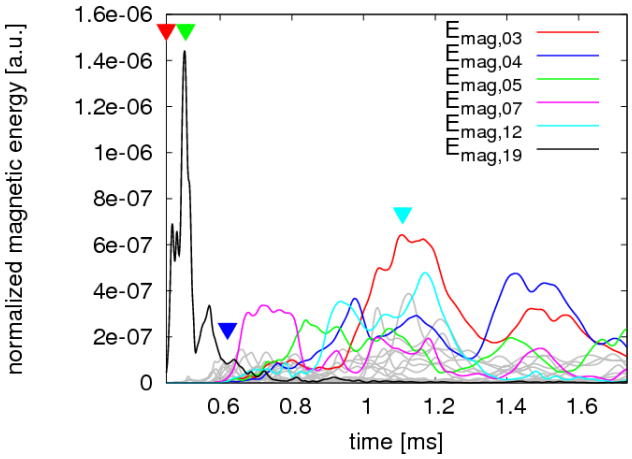

Figure 1: *Time-trace of normalized magnetic energy for different toroidal harmonics during the ELM crash*

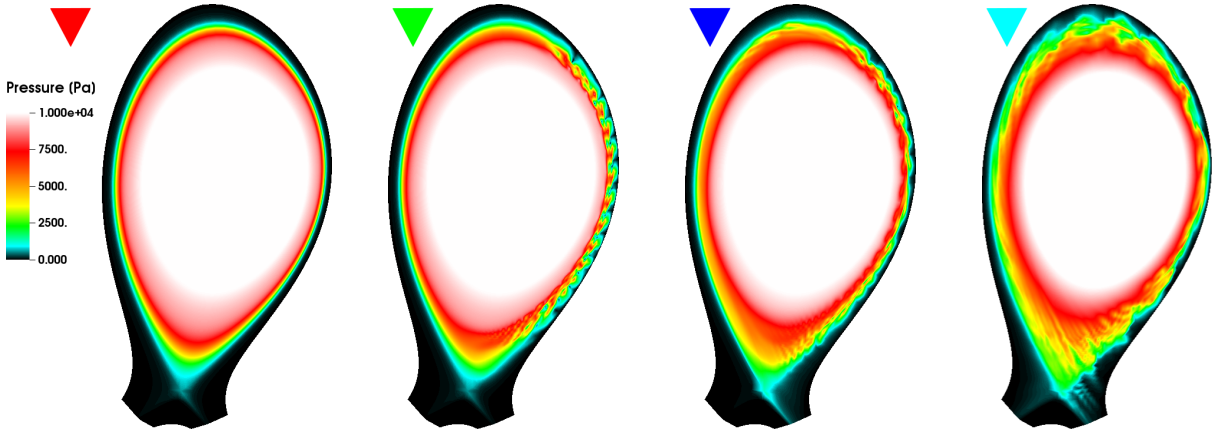

Figure 2: *Pressure distribution in the poloidal plane during the ELM crash*

intermediate and low mode numbers become more and more important. Similar transitions of high-n to low-n components have also been observed experimentally [5, 6] and are driven by quadratic mode coupling [7].

Figure 2 shows the pressure distribution in the poloidal plane at four different points in time which are indicated by colored triangles in figure 1. The evolution of the pressure profile in the pedestal region (outward midplane) is shown in figure 3 using a coloring corresponding to the triangles in figures 1 and 2, respectively. One

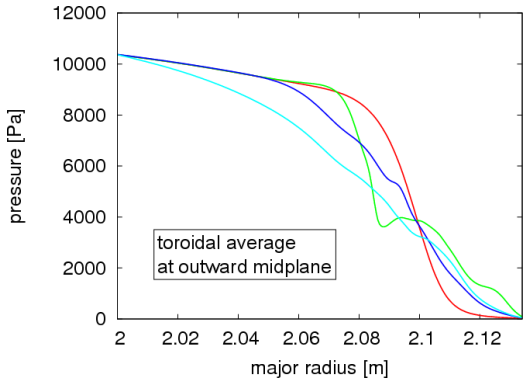

Figure 3: *Pedestal collapse during the ELM crash*

can clearly see how the pedestal collapses at the onset of the ELM and eventually flattens as the crash continues. Again this is in qualitative agreement with experimental findings [8]. Unfortunately, the pedestal does not build back up again in the simulation. Instead we observe continuous strong magnetic activity ('ballooning turbulence') after the crash (see figures 1 and 2) which prevents the pedestal from recovering.

Diamagnetic Stabilization

In this section we show first results regarding simulations of ELMs in AUG including diamagnetic drift effects. The simulations are based on AUG discharge #23221@4.25s with a core resistivity of 7.5×10^{-7} Ωm. In order to study the influence of the diamagnetic terms on the toroidal mode spectrum we have performed several quasi-linear runs including only a single toroidal harmonic and mode numbers ranging from $n = 2$ to $n = 20$. Figure 4 shows the linear growth rate of the instability versus mode number both with ($\tau_{\mathrm{IC}} = 5 \times 10^{-3}$) and without ($\tau_{\mathrm{IC}} = 0$) diamagnetic drift effects as well as for an intermediate value of the diamagnetic parameter ($\tau_{\mathrm{IC}} = 2 \times 10^{-3}$). One can clearly see a stabilization of high-n components through the diamagnetic drift terms leading to a maximum of the growth rate at intermediate mode numbers. This is in qualitative agreement with experimental observations [11]. The simulations above have been conducted with an intermediate resolution of the poloidal grid. In order to estimate the error bars in the plot, we have performed resolution scans of the growth rate of the individual toroidal harmonics for $\tau_{\mathrm{IC}} = 0$ and $\tau_{\mathrm{IC}} = 5 \times 10^{-3}$ as shown in figure 5. The growth

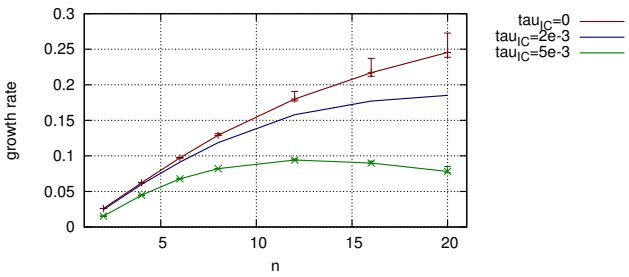

Figure 4: *Diamagnetic stabilization of high-n components*

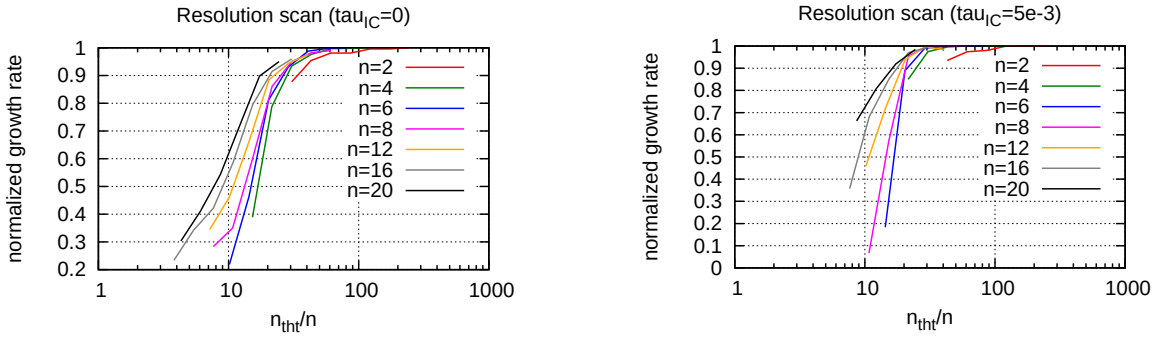

Figure 5: *Resolution scan with and without diamagnetic drift effects for different toroidal harmonics*

rates have been normalized to their saturation value and plotted against the number of poloidal grid points divided by the mode number. This choice seems reasonable since, although radial and poloidal resolution of the grid have been varied simultaneously, the poloidal resolution is the limiting one due to the fine filamentary structures whose typical length scale is inversely proportional to the mode number. Consequently high mode numbers are difficult to resolve as is clearly visible from the plot.

Figure 6 shows two simulations of a full ELM crash (for simplicity including only $n = 8$) with and without diamagnetic drift effects. In the former case, the ballooning turbulence is clearly suppressed which is a key ingredient for the simulation of ELM cycles [9].

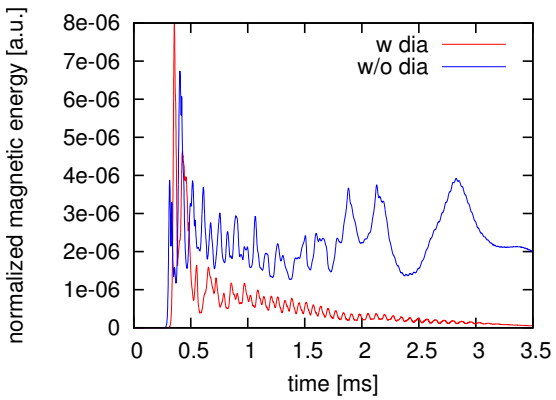

Figure 6: *Suppression of ballooning turbulence*

Summary and Outlook

We have performed simulations of full ELM crashes in AUG with and without diamagnetic drift effects. The simulations without diamagnetic drift are in qualitative agreement with experimental findings regarding the evolution of toroidal Fourier spectrum and pedestal. However, multi-ELM simulations are not possible due to a persistent ballooning turbulence after the first crash. Simulations including diamagnetic drift effects have confirmed the stabilization of high toroidal mode numbers as well as the suppression of ballooning turbulence after the first crash. They are thus a key ingredient for multi-ELM simulations.

Next steps will be to perform multi-ELM simulations for AUG as well as to include and verify a model for a consistent bootstrap current which has recently been implemented in JOREK [10]. On the long term we aim to identify different ELM types as observed in experiments [11] and to compare the results to experimental observations, e.g., regarding pedestal evolution and heat deposition patterns.

Acknowledgments

This work has been carried out within the framework of the EUROfusion Consortium and has received funding from the Euratom research and training programme 2014-2018 under grant agreement number 633053. The views and opinions expressed herein do not necessarily reflect those of the European Commission.

References

[1] F. Orain et al., Phys Plasmas **20**, 102510 (2013)
[2] G. Huysmans et al., Nucl Fusion **47**, 659 (2007)
[3] O. Czarny et al., J Comput Phys **227**, 7423 (2008)
[4] M. Dunne, private communication (2014)
[5] J. E. Boom et al., Nucl Fusion **51**, 103039 (2011)
[6] R. P. Wenninger et al., Nucl Fusion **53**, 113004 (2013)
[7] I. Krebs et al., Phys Plasmas **20**, 082506 (2013)
[8] P. Schneider et al., Plasma Phys Control Fusion **56**, 025011 (2014)
[9] F. Orain et al., Plasma Phys Control Fusion **57**, 014020 (2015)
[10] S. Pamela, Invited talk at EPS 2015, Lisbon (2015)
[11] H. Zohm, Plasma Phys Control Fusion **38**, 105 (1996)